inventions

MDPI

Article

Design and Simulation of a Greenhouse FSS Nanofiber Film for Enhancing Agricultural Productivity by Selective Reduction of UV and NIR

Abhisit Sripradit and Thorin Theeradejvanichkul *

Department of Electronic and Telecommunication Engineering, Faculty of Engineering, King Mongkut's University of Technology Thonburi, Bangkok 10140, Thailand; abhisit.sri@mail.kmutt.ac.th
* Correspondence: thorin.the@kmutt.ac.th

Abstract: A greenhouse covering film is an essential part of any greenhouse. Its function is to filter solar radiation in the ultraviolet (UV) and the near-infrared (NIR) bands while allowing a great amount of photosynthetically active radiation (PAR) to transmit. This paper proposes a design of the greenhouse covering film based on a frequency selective surface (FSS). Aluminum is made into fibers in the nanoscale. They are laid out in an array, in-plane at equidistance from one another. This arrangement induces the wavelength selectivity of light via adjustment to the fiber sizes and spacings. The performance is evaluated by a finite element analysis (FEA) method. The results show less than 26% transmittance of UV and NIR while allowing more than 94% transmittance in the PAR regime.

Keywords: finite element analysis; FEA; frequency selective surface; FSS; greenhouse covering film; Gaussian mixture models; GMMs; near-infrared; NIR; photosynthetically active radiation; PAR; polyethylene terephthalate; PET; ultraviolet; UV

Citation: Sripradit, A.; Theeradejvanichkul, T. Design and Simulation of a Greenhouse FSS Nanofiber Film for Enhancing Agricultural Productivity by Selective Reduction of UV and NIR. *Inventions* **2022**, *7*, 16. https://doi.org/10.3390/inventions7010016

Academic Editors: Goshtasp Cheraghian and Monique Lacroix

Received: 24 October 2021
Accepted: 8 January 2022
Published: 26 January 2022

Publisher's Note: MDPI stays neutral with regard to jurisdictional claims in published maps and institutional affiliations.

1. Introduction

Greenhouse and film technology have converged and evolved significantly over the last decade. A greenhouse enables crop cultivation in a controlled environment or in a region where weather conditions are unrelenting, such as broad temperature fluctuation, heavy rain, strong winds, arid conditions, or pests and diseases [1–3]. One of the most critical parts of a greenhouse is the covering film [4]. The film is designed to increase agricultural productivity by reducing ultraviolet (UV-A: 320–400 nm and UV-B: 290–320 nm) [5] and near-infrared (NIR: 700–1500 nm) [6] radiation from the sun, as UV and NIR are responsible for increasing pests. Hence, we can increase agricultural productivity by reducing UV and NIR.

Conventional greenhouse covering film technology can be divided into five groups, as shown in Figure 1. The first is chemical coating. Hemming et al. presented the whitewash solution ($Ca(OH)_2$) as a coating agent to reduce NIR by reflection [3,7]. Although $Ca(OH)_2$ can significantly reduce the amount of NIR radiated into the greenhouse, $Ca(OH)_2$ decreases PAR by a more significant proportion than the amount of NIR reduction. Furthermore, a drawback of using chemical coatings is that they deteriorate and degrade the NIR and UV protection capacity when exposed to the environment [8]. The second and third groups are metal oxides and metal compounds, respectively. Black iron oxide and blue cobalt oxide can reduce UV transmission by 53% and reflect 14% of the NIR, but the PAR level is also reduced down to 43% [9] as a drawback. The metal compounds used to replace metal oxide in the previous group are CoAl, CoNiZnTi, CrSbTi, MnSbTi, and NiSbTi. The fourth group uses polymers such as polyvinyl chloride (PVC), acrylic, D-polymer, linear low-density polyethylene (LLDPE), and polyolefins [10]. Polymers are often used as the primary material of the greenhouse covering film because they have desirable optical

properties that allow light to transmit through and reduce the amount of UV and NIR via the transmission and reflection properties of the films.

Finally, the last group uses metal nanoparticles such as titanium dioxide, silicon oxide, and zinc oxide. The absorption and reflection can be controlled by the particle size [9]. Solovyev et al. proposed a design of a multilayer low-emissivity (low-E) coating on polyethylene terephthalate (PET) and polyethylene (PE) films [11]. The TiO_2/ZnO: Ga/Ag/ZnO: Ga/TiO_2 coating has 82% transmission of the PAR and 91% reflection of the NIR. This group uses noble elements such as gallium (Ga), silver (Ag), and titanium (Ti). Titanium dioxide is a commonly used primary material in this group [3,12–14]. Although they enhance the NIR reflectivity, it is preferable to use inexpensive materials such as aluminum (Al) instead of noble elements like titanium. In 2019, Petchsuk et al. developed a UV-blocking material using TiO_2-78% anatase and TiO_2-100% rutile for a greenhouse covering application [9]. However, nanoparticles in this group may suffer two drawbacks: photodegradation and transparency loss [15].

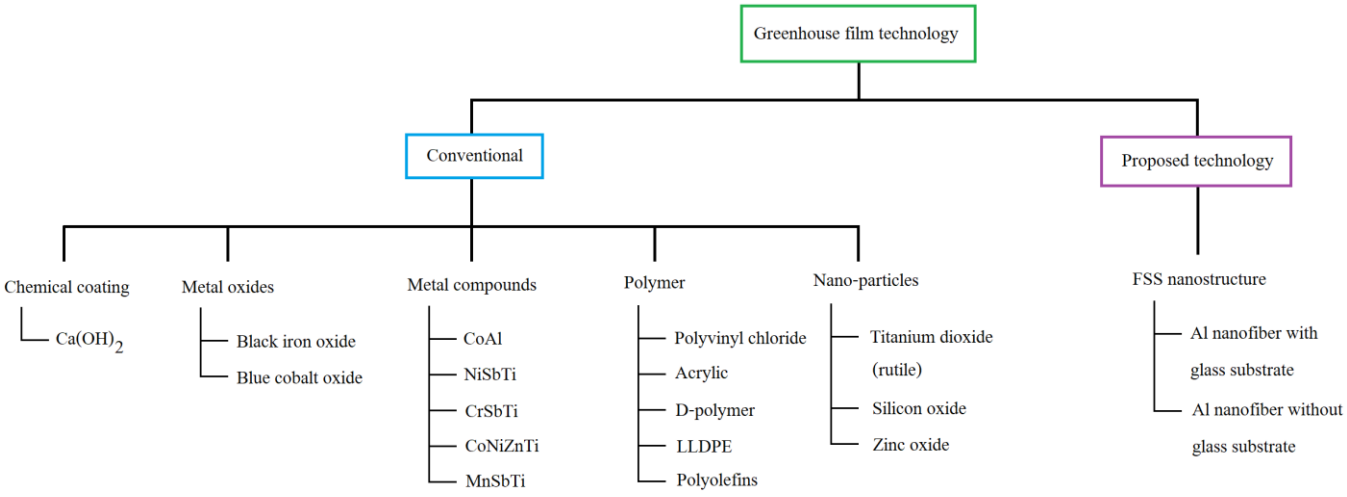

Figure 1. Greenhouse covering film technology.

Conventional method relies on "trial and error" and repeatedly testing the material to find the best result rather than optimizing the structure to design a new material. This method is expensive and time-consuming. Nevertheless, these shortcomings can be eliminated by computer modeling via a finite element analysis (FEA) method. FEA averts the use of actual materials for experimentation and provides an in-depth analysis of the film structure in nanoscale. FEA opens up new possibilities for increased performance, durability, and optimization. It also reduces the cost of mass prototyping to find the best solution because we can immediately adjust the film's structure and composition on a computer.

In this paper, we present a design of a greenhouse covering film based on a frequency selective surface (FSS) nanostructure [16]. The film contains aluminum fibers that are nanometer in size and structurally capable of filtering out UV and NIR. The fibers are assembled with two options: PET with glass and PET without glass. FEA evaluates the film performance.

The paper is organized as follows. Section 1 introduces background of the conventional greenhouse covering film technology previously reported as five groups: chemical coating, metal oxides, metal compounds, polymers, and nanoparticles. Section 2 describes the design principles of the proposed greenhouse covering film and the simulation domain setup. Section 3 discusses results from the parametric studies of the nanofiber when surrounded by PET. It also investigates the effects of nanofiber size and substrate component on the transmittance of NIR, PAR, and UV. Validation of the results will also be discussed. Finally, Section 4 concludes.

2. Materials and Methods

Our research focuses on using low-cost material with novel technology. From the literature review, PET and Al are good material choices for the design of greenhouse covering film. Some studies show that glass with a coating material is suitable for greenhouses covering material [17]. Hence, we propose to investigate the covering films, with (and without) a glass substrate.

2.1. Design of Nanofiber Film

The proposed film depicted in Figure 2 can be designed with (or without) a glass substrate. Instead of relying on the material's properties alone, we take advantage of the periodicity in the fiber arrangement to induce the frequency selective behavior of the film, providing the fiber dimension is of the same order of magnitude as the wavelength of interest. The film is made of transparent and pliable polymers such as polyethylene terephthalate (PET). Inside, there are many nanofibers that lie in a two-dimensional plane and sandwiched between two layers of PET. These nanofibers can filter out unwanted UV and NIR and allow PAR light to pass through if the size of the nanofiber is properly designed. The spacing between the metal strips is filled with PET. The film composite structure in Figure 2 can be manufactured by roll-to-roll nano-imprint lithography at approximately $12 per square meter [18].

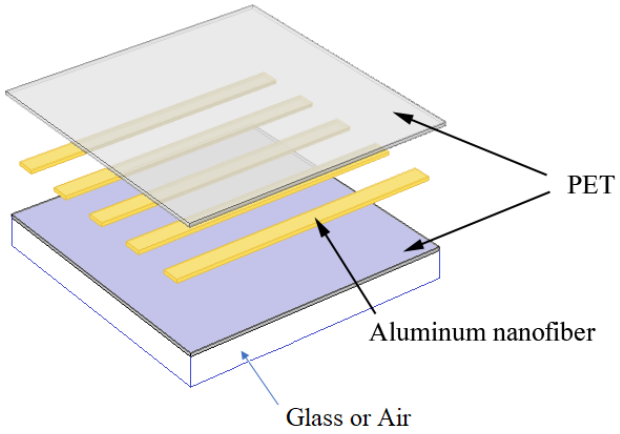

Figure 2. Proposed nanofiber film.

2.2. Evaluation and Domain Setup

The finite element analysis (FEA) method is a powerful and commonly used tool to model and analyze complex structures. Structural design of filter film with FEA requires boundary conditions to determine the characteristics of the simulating device. In this paper, we use aluminum, PET, and glass as the primary materials for the film. A perfect electric conductor (PEC) is a popular boundary condition preferred to model metallic materials such as copper. Using the perfect electric conductor boundary condition for a metal, however, would put the metal we are analyzing in its perfect conductor, of which characteristics can deviate from the those of the metal (imperfect electric conductor). It may give rise to inconsistent results with the actual experimental results because the true metallic properties of metals do change with the wavelength, in a nonlinear fashion. Therefore, to get results as close to reality as possible, we need to use the actual properties of the metals in FEA. In the NIR-PAR-UV regime, the nonlinear optical properties of materials are obtained from [19–21].

To control the transmission or rejection of NIR-PAR-UV, we have to design the nanometer-scale structure of the film as a frequency selective surface (FSS). Such a surface is a periodic structure in which there is a large number of repeating unit cells in two dimensions. Hence, to create the conditions of the FSS, we define the boundaries of unit cell sides as periodic [22,23].

The characteristics of FSS can be affected by the physical parameters such as the width and height of the nanostructure, the constitutive parameters from the optical properties of the materials, and the incident angle. Almost all greenhouses are of the Quonset-type shown in Figure 3a. The sunray is assumed to always be perpendicular (or at normal incidence) to the film's surface [24], as in Figure 3b, with an input power of one watt. After designing the nanostructures of the film with periodic boundary condition, FEA solves Maxwell's equations to simulate the film characteristics based on the constitutive properties of materials [22].

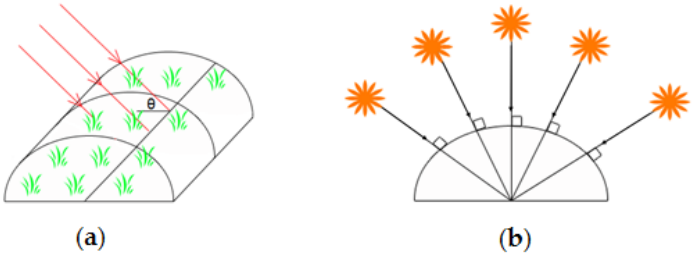

Figure 3. (**a**) Sunrays incident upon a Quonset-type greenhouse. (**b**) Sunray is assumed to be perpendicular to the Quonset-type surface.

In Figure 4, illumination of light starts from the junction area between the perfectly matched layers and the upper air layer down to the film. Al nanofibers are sealed on top with PET. The air layer encloses the film surrounding a perfectly matched layer boundary condition for absorbing all reflected waves, assuming that the top and bottom regions of the film are infinite in extent [22]. The PML layers have a height of 33 µm. All domains are meshed by tetrahedral meshes, as in Figure 5, with a maximum size of no more than 0.6 times the shortest PAR wavelength (or in this case 0.6 × 400 nm). In our study, the largest mesh size is no more than 240 nm.

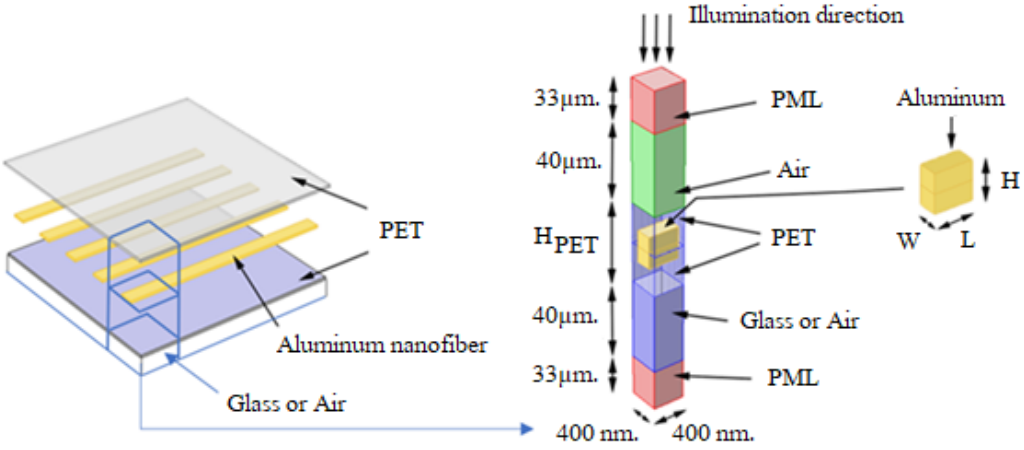

Figure 4. Domain and boundary setup of the proposed film.

In this research, parametric studies are the following:

1. Width (W) of the nanofiber in the range from 100 nm to 300 nm.
2. Height (H) of the nanofiber in the range from 10 nm to 1000 nm.

The parametric studies start with a step adjustment of the fiber dimension on two variables: the width (W) and the height (H) of the nanofiber. Those parameters would affect the proposed film in terms of the transmittance in the UV-PAR-NIR regimes. A desirable film would allow transmission of PAR while blocking the UV and NIR transmission. An optimal dimension of the nanofibers is found from trading off some level of the PAR for the reduction of UV and NIR transmission. Outputs of the simulation are S-parameters such as transmission and reflection coefficients, which indicate the efficiency of the proposed film.

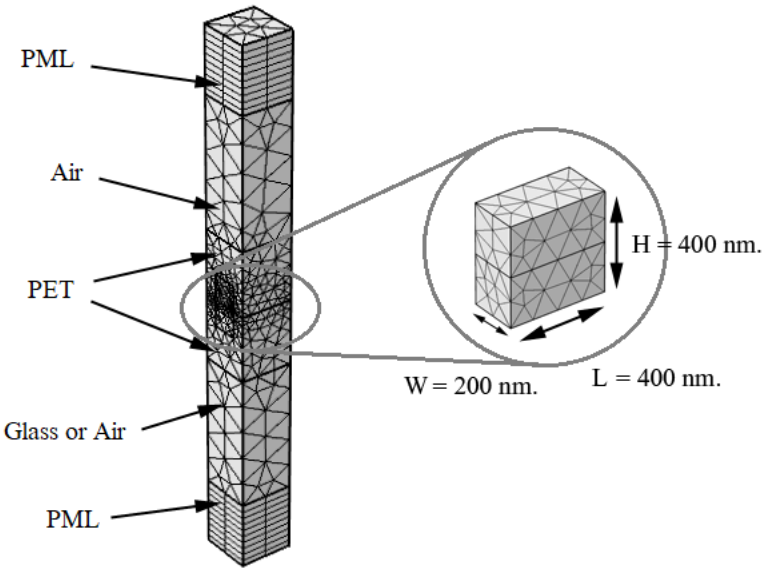

Figure 5. Meshing characteristics of the proposed film.

3. Results and Discussion

The results obtained from FEA are presented in the form of a distribution of transmittance over wavelengths. We discuss a regression analysis to model this distribution with a mathematical equation. Such an equation would allow us to understand the selectivity behavior of the proposed film in terms of critical statistical quantities, such as the mean and the standard deviation, which make it simpler to formulate the transmittance in the desired frequency band.

3.1. Width of the Nanofiber (W)

Figure 6 demonstrates that, at a wavelength less than 400 nm, varying W does not affect the transmittance too significantly. The transmittance curves appear to be overlapping and do not differ much from one another. At a wavelength of more than 400 nm, the transmittance decreases substantially, rendering less NIR transmission. The PAR transmittance starts to decrease if W is more than 200 nm. For W less than 200 nm, PAR is slightly increased, whereas NIR is significantly increased. Reducing W further would see a more pronounced tradeoff between the PAR and the NIR levels. Therefore, W = 200 nm is chosen as the value of choice for the subsequent studies.

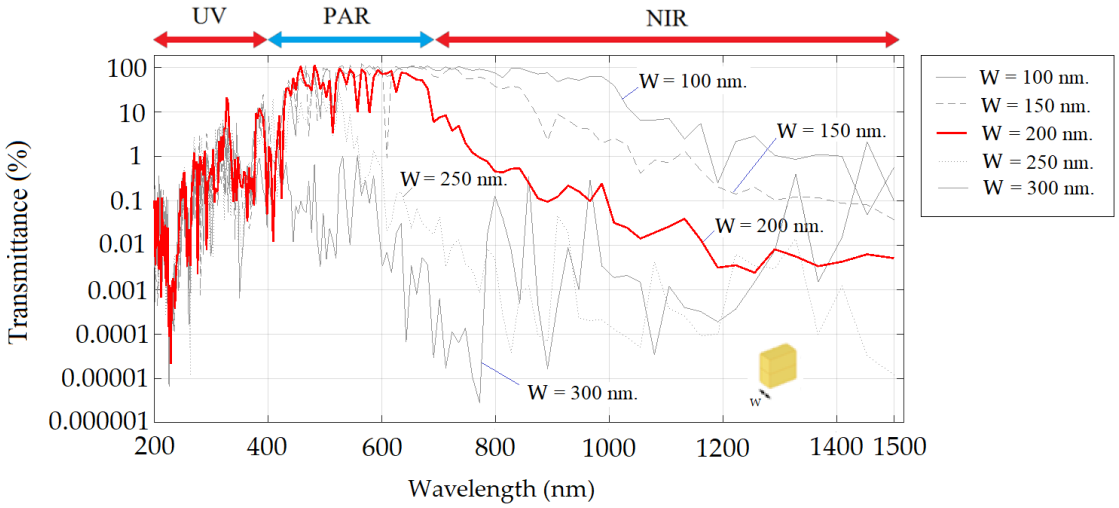

Figure 6. Transmittance when W is varied from 100 nm to 300 nm.

3.2. Height of the Nanofiber (H)

Height (H) is varied from 10 nm to 1000 nm with an increment of 10 nm in the range from 10 nm to 100 nm and 100 nm in the others. Results are shown in Figure 7 (with some H values omitted for clarity). The results show overlapping lines in the 200–450 nm range for all H variations. At the wavelength of 600 nm or more, the transmittance has a downward trend as H is varied. The results imply a reduction of NIR level. In the UV regime, the transmittance also exhibits a downward trend, indicating the film's ability to block UV. It is found that when H is more than 400 nm, the transmittance of PAR starts to decrease. If H is less than 400 nm, PAR will slightly increase, but the trade-off with an increasing level of NIR would be too unfavorable. That is why H = 400 nm is chosen.

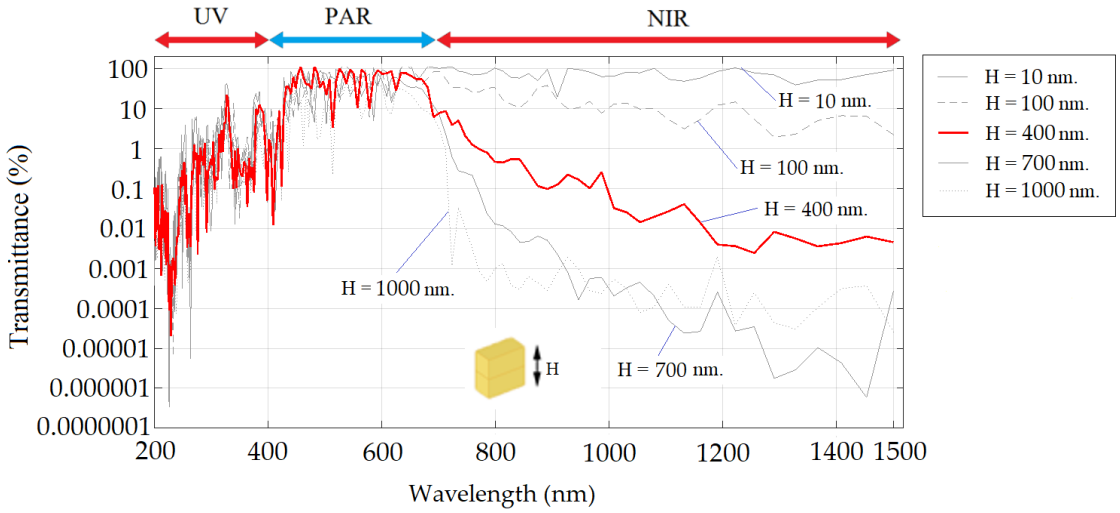

Figure 7. Transmittance when H is varied from 10 nm to 1000 nm.

The results of the proposed film with a glass layer are similar to the ones without it. This demonstrates that the proposed film has flexibility in implementation to retain the filtration ability. The most proper dimensions of W and H are 200 nm and 400 nm, respectively. The results for both films, with and without the glass layer, are shown in Figure 8.

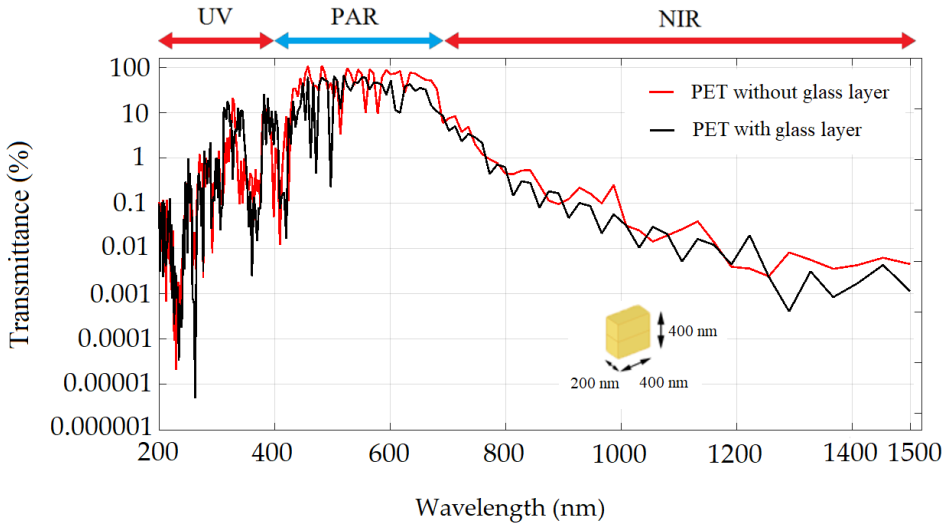

Figure 8. The transmittance of a film (with and without a glass layer).

3.3. Validation of the Results

To validate the results, we compare ours with seven independently reported experimental results by other researchers [25–31]. In 2017, Xie et al. [25] presented a prototype made of aluminum nanofibers (W = 150 nm, H = 90 nm). Their experiment showed that the fabricated prototype exhibited 10–40% transmittance in the PAR regime. Such findings are consistent with our simulation results and those of the other six experimental results, under the same fiber dimensions, as shown in Figures 9–11 and Table 1.

Wu et al. [29], Chen et al. [30], and Ahn et al. [31] built and tested their aluminum nanofiber with different sizes. Wu et al. (W = 107 nm and H = 145 nm) tested their prototypes at 635 nm. Their nanofiber delivered 61% transmittance, whereas ours is at 51.78%. Chen et al. (W = 47 nm and H = 177 nm) performed experiments at two wavelengths: 450 and 550 nm. The transmittances were found to be at 76% and 79%, whereas ours are at 80.59% and 73.15%, respectively. Finally, Ahn et al. (W = 50 nm and H = 200 nm) measured 85% transmittance at 450 nm, compared to ours at 80.54%. Table 1 summarizes the result validation with other published experimental results.

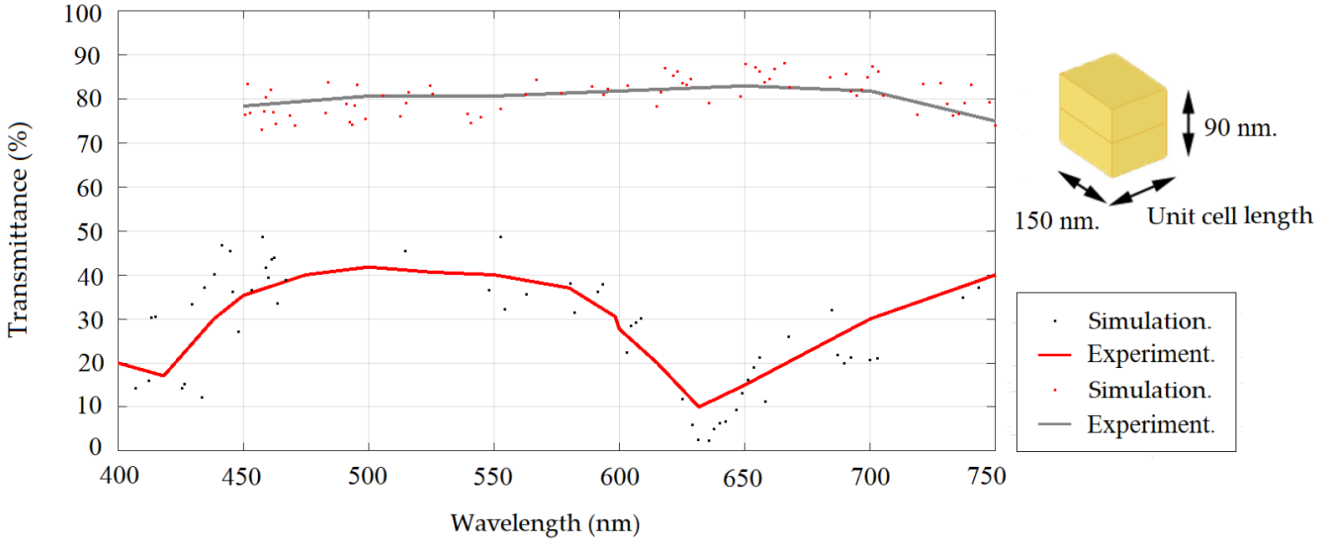

Figure 9. Comparison of our simulation and experimental results [25,28] using Al fiber (W = 150 nm, H = 90 nm and W = 70 nm, H = 200 nm, respectively).

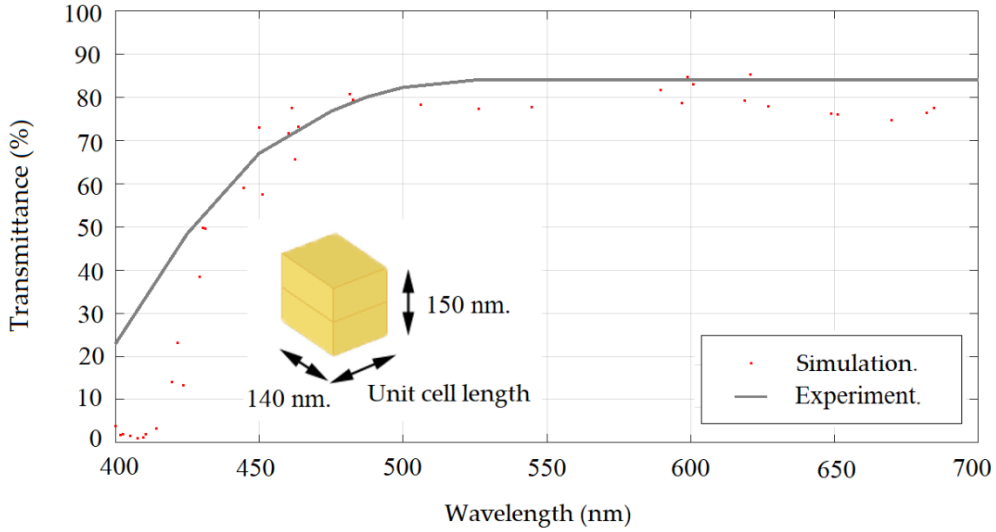

Figure 10. Comparison of our simulation and experimental results [26] using Al fiber (W = 140 nm and H = 150 nm).

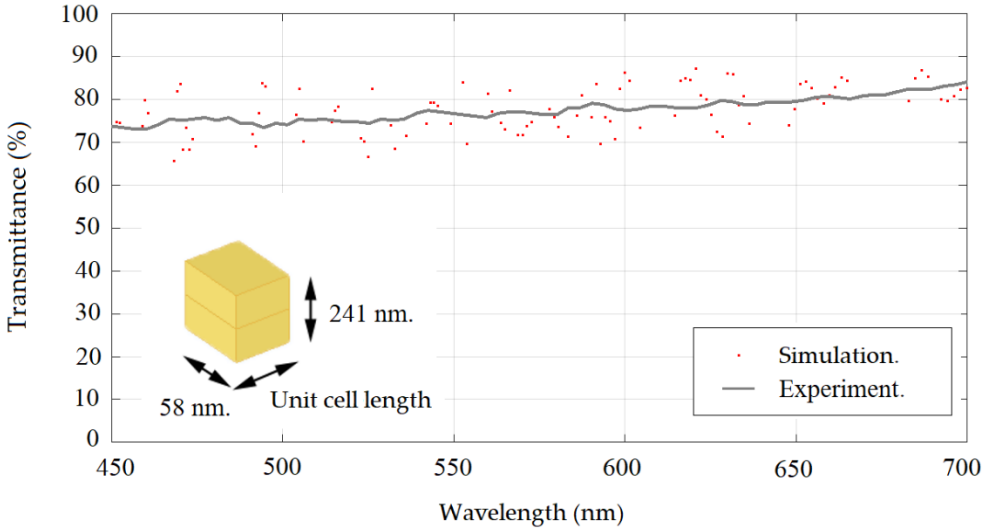

Figure 11. Comparison of our simulation and experimental results [27] using Al fiber (W = 58 nm and H = 241 nm).

Table 1. The conclusion of comparison of our simulation with the experimental results.

Ref.	W (nm)	H (nm)	% Transmittance (Experiment)	% Transmittance (Simulation)	Wavelength (nm)	Difference (%)
[25]	150	90	Figure 9	Figure 9	Figure 9	-
[26]	70	200	Figure 10	Figure 10	Figure 10	-
[27]	140	150	Figure 11	Figure 11	Figure 11	-
[28]	58	241	Figure 9	Figure 9	Figure 9	-
[29]	107	145	61	51.78	635	15.11
[30]	47	177	76	80.59	450	6.04
[30]	47	177	79	73.15	550	7.41
[31]	50	200	85	80.54	450	5.25

Although all results are consistent, Xie's prototype and the others. however, are not suitable for greenhouse covering films because they are not optimized to filter out the UV and the NIR. Figures 6 and 7 show that the film cannot reject the NIR when W < 100 nm and H > 400 nm. The best fiber dimension is determined from our studies, specifically, W = 200 nm and H = 400 nm.

3.4. The Regression Analysis

The goal in this section is to find a correlation equation of the transmittance obtained from the simulations. Such an equation allows us to estimate the transmittance at various wavelengths without the need for repeated simulations. The transmittance data obtained from the simulation are shown in Figure 12.

As the curve has a bell-shape right-skewed Gaussian distribution, we will use Gaussian mixture models (GMMs) to model it. The GMMs equation of the transmittance (τ) as a function of wavelength (λ) and the number of peaks to fit (n) is the following:

$$\tau = \sum_{i=1}^{n} a_i e^{-\left(\frac{\lambda - b_i}{c_i}\right)^2} \quad (1)$$

For the Gaussian regression at $n = 3$, the curve resembles the original data more closely than $n = 2$. The characteristic of the graph fits nicely on the data in the 800–1200 nm regimes. Therefore, the equation with $n = 3$ is suitable for predicting the transmittance. The Gaussian regression coefficients are tabulated in Table 2.

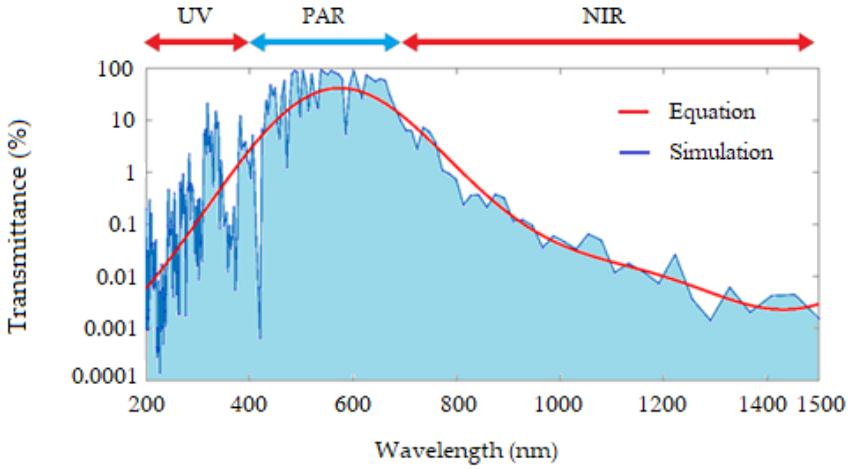

Figure 12. Gaussian regression of transmittance (W = 200 nm, H = 400 nm). (The area under curve is provided for visual clarity.)

Table 2. The transmittance coefficients by Gaussian regression at n = 3.

a_1	$\mathbf{b_1}$	$\mathbf{c_1}$	a_2	$\mathbf{b_2}$	$\mathbf{c_2}$	a_3	$\mathbf{b_3}$	$\mathbf{c_3}$
44.7	549.7	327.3	−13.3	1462	238.8	−3599	−19,680	9754

In Table 2, a_1 is the level of transmitted light at a wavelength of interest; $\mathbf{b_1}$ indicates the mean or the center wavelength of the selectivity passband; $\mathbf{c_1}$ indicates the standard deviation of the wavelength to pass. In the case of the proposed film, $\mathbf{b_1}$ is 549.7, and $\mathbf{c_1}$ is 327.3. It simply means that the proposed film allows the wave at 549.7 nm to pass with standard deviation in wavelength of $327.3/\sqrt{2}$ nm. In other words, the proposed film has transmission in the PAR regime, going from λ = 549.7–$327.3/\sqrt{2}$ = 318.26 nm to 549.7 + $327.3/\sqrt{2}$ = 781.13 nm.

Because the simulation curve is not a perfect Gaussian distribution, we need to add the higher order terms: a_2, $\mathbf{b_2}$, $\mathbf{c_2}$, a_3, $\mathbf{b_3}$, and $\mathbf{c_3}$, to better fit the Gaussian model to the simulation data. The transmittance can be determined from:

$$\text{Transmittance } (\%) = 10^{2+0.1\tau} \tag{2}$$

where τ is the transmittance (in dB). The corresponding reflectance (%) can be determined from 100%–transmittance (%).

The summit of the curve shown in Figure 10 occurs at λ of 564 nm. At such a wavelength, the simulation data yield a transmittance of 94.87% or −0.22851 dB. In contrast, the GMMs curve predicts the transmittance of −3.8527 dB. Therefore, the GMMs curve and the simulation curve still differ from each other. Hence, we need to adjust the offset to nullify this difference, resulting in transmittance equation:

$$\text{Transmittance } (\%) = 10^k; k = 2 + 0.1\left(44.7e^{-\left(\frac{\lambda-549.7}{327.3}\right)^2} - 13.3e^{-\left(\frac{\lambda-1462}{238.8}\right)^2} - 3599e^{-\left(\frac{\lambda+19680}{9754}\right)^2} + 3.6205\right) \tag{3}$$

Equation (3) is the formula used to evaluate the efficiency of greenhouse covering film in terms of transmittance of wave at a wavelength of interest. It yields a maximum transmittance of 94.79% at wavelength of 564 nm (approximately center of PAR regime) and less than 26% in UV and NIR regimes. The proposed film performs better than [9] and [11] in terms of its selective transmission.

4. Conclusions and Future Work

This paper presents a new design of a greenhouse covering film, capable of filtering out UV and NIR while allowing PAR to pass through. FSS aluminum nanofibers are utilized

for the design. The fibers are assembled on two substrate options: PET with glass and PET without glass. Both are also coated with PET on top. FEA technique is used to evaluate the performance of the proposed FSS greenhouse film.

From the parametric studies, it is found that increasing width (W) and height (H) of the nanofiber can reduce the transmission of NIR. Optimal nanofiber sizes that protect against UV and NIR but still provide good PAR throughput are obtained by a trade-off between the amount of PAR being reduced and the UV and NIR shielding. When W is greater than 200 nm and H is greater than 400 nm, the resulting UV and NIR protection is not worth the drastic reduction in PAR. It is ineffective when used as a greenhouse covering film because plants will not have light for photosynthesis.

The film's best performance shows less than 26% transmittance (or more than 74% rejection) of UV and NIR while allowing more than 94% transmittance of the PAR. We also compared our results to seven other independent published research studies that fabricated nanofibers with the same material (aluminum) ranging in size from 10 nm to 400 nm. Our results are consistent with those studies. Furthermore, we can use the Gaussian mixture models to model the transmittance of the FSS film. Thus, it helps those who are interested in designing FSS nanofiber greenhouse film to estimate its wavelength selectivity. Additionally, to bring it to industrial use, the authors plan to study the effect of incident angle on filtration selectivity and to fabricate an actual nanofiber film by the technique of roll-to-roll nano-imprint lithography.

Author Contributions: Conceptualization, A.S. and T.T.; methodology, A.S. and T.T.; validation, A.S.; formal analysis, A.S.; investigation, A.S.; writing—original draft preparation, A.S. and T.T.; writing—review and editing, A.S. and T.T.; visualization, A.S. and T.T.; supervision, T.T.; project administration, T.T.; data curation, T.T.; funding acquisition, T.T. All authors have read and agreed to the published version of the manuscript.

Funding: This research received no external funding.

Acknowledgments: The authors wish to express their gratitude toward IoT Lab, Department of Electronic and Telecommunication Engineering, Faculty of Engineering, King Mongkut's University of Technology Thonburi, Bangkok, Thailand, for their support.

Conflicts of Interest: The authors declare no conflict of interest.

Abbreviations

BPF	Band-pass filter
FEA	Finite element analysis
FSS	Frequency selective surface
GMMs	Gaussian mixture models
LLDPE	Linear low-density polyethylene
Low-E	Low-emissivity
NIR	Near-infrared
PML	Perfectly matched layer
PAR	Photosynthetically active radiation
PE	Polyethylene
PET	Polyethylene terephthalate
PVC	Polyvinyl chloride
UV	Ultraviolet

References

1. Kumar, K.; Tiwari, K.; Jha, M.K. Design and technology for greenhouse cooling in tropical and subtropical regions: A review. *Energy Build.* **2009**, *41*, 1269–1275. [CrossRef]
2. Behn, H.; Tittmann, S.; Walter, A.; Schurr, U.; Noga, G.; Ulbrich, A. UV-B transmission of greenhouse covering materials affects growth and flavonoid content of lettuce seedlings. *Eur. J. Hortic. Sci.* **2010**, *75*, 259–268.

3. Abdel-Ghany, A.M.; Al-Helal, I.M.; Alzahrani, S.M.; Alsadon, A.A.; Ali, I.M.; Elleithy, R.M. Covering Materials Incorporating Radiation-Preventing Techniques to Meet Greenhouse Cooling Challenges in Arid Regions: A Review. *Sci. World J.* **2012**, *2012*, 1–11. [CrossRef]
4. Dehbi, A.; Mourad, A.-H.I. Durability of mono-layer versus tri-layers LDPE films used as greenhouse cover: Comparative study. *Arab. J. Chem.* **2016**, *9*, S282–S289. [CrossRef]
5. Chen, P.; Liu, T.; Wang, D.; Zhang, Q.; Hu, L. Modified Vinyl–POSS Materials as Sun Protection Factor and as Films for Greenhouse Cover. *Ferroelectrics* **2010**, *411*, 36–43. [CrossRef]
6. Yang, X.; Miller, D.R. Calculation of Potential Broadband Biologically Active and Thermal Solar Radiation above Vegetation Canopies. *J. Appl. Meteorol.* **1995**, *34*, 861–872. [CrossRef]
7. Hemming, S.; Kempkes, F.; Van Der Braak, N.; Dueck, T.; Marissen, N. Greenhouse Cooling by Nir-Reflection. *Acta Hortic.* **2006**, *719*, 97–106. [CrossRef]
8. Dehbi, A.; Mourad, A.-H.I.; Djakhdane, K.; Hilal-Alnaqbi, A. Degradation of thermomechanical performance and lifetime estimation of multilayer greenhouse polyethylene films under simulated climatic conditions. *Polym. Eng. Sci.* **2014**, *55*, 287–298. [CrossRef]
9. Petchsuk, A.; Srinun, D.; Buchatip, S.; Supmak, W.; Sirikittikul, D. Development of Multifunctional Film for Greenhouse Applications in Tropical Regions. *Adv. Mater. Sci. Eng.* **2019**, *2019*, 1692126. [CrossRef]
10. Maraveas, C. Environmental Sustainability of Greenhouse Covering Materials. *Sustainability* **2019**, *11*, 6129. [CrossRef]
11. Solovyev, A.; Rabotkin, S.; Kovsharov, N. Polymer films with multilayer low-E coatings. *Mater. Sci. Semicond. Process.* **2015**, *38*, 373–380. [CrossRef]
12. Sánchez, V.H.; López, R.; Ramón, G.M.; Enríquez-Pérez, A.; Camacho-López, M.; Villa-Sánchez, G. Annealing Control on the Anatase/Rutile Ratio of Nanostructured Titanium Dioxide Obtained by Sol-Gel. *Crystals* **2018**, *9*, 22. [CrossRef]
13. Lu, P.J.; Fang, S.W.; Cheng, W.L.; Huang, S.C.; Huang, M.C.; Cheng, H.F. Characterization of titanium dioxide and zinc oxide nanoparticles in sunscreen powder by comparing different measurement methods. *J. Food Drug Anal.* **2018**, *26*, 1192–1200. [CrossRef] [PubMed]
14. Kang, X.; Liu, S.; Dai, Z.; He, Y.; Song, X.; Tan, Z. Titanium Dioxide: From Engineering to Applications. *Crystals* **2019**, *9*, 191. [CrossRef]
15. Espejo, C.; Arribas, A.; Monzó, F.; Díez, P. Nanocomposite films with enhanced radiometric properties for greenhouse covering applications. *J. Plast. Film. Sheeting* **2012**, *28*, 336–350. [CrossRef]
16. Sripradit, A.; Theeradejvanichkul, T. A frequency selective surface with nano square ring resonators for enhancing banknote security. In Proceedings of the 2017 IEEE International Symposium on Antennas and Propagation USNC/URSI National Radio Science Meeting, San Diego, CA, USA, 9–14 July 2017; pp. 677–678.
17. Max, J.F.; Reisinger, G.; Hofmann, T.; Hinken, J.; Tantau, H.-J.; Ulbrich, A.; Lambrecht, S.; Von Elsner, B.; Schurr, U. Glass–film-combination: Opto-physical properties and energy saving potential of a novel greenhouse glazing system. *Energy Build.* **2012**, *50*, 298–307. [CrossRef]
18. Toor, F.; Guneratne, A.C.; Temchenko, M. Metal-dielectric frequency-selective surface for high performance solar window coatings. *Photonic Phononic Prop. Eng. Nanostruct. VI* **2016**, *9756*, 97561S.
19. Refractive Index Database. Available online: https://refractiveindex.info/?shelf=mainbook=Alpage=Rakic (accessed on 4 December 2017).
20. Hong, N.; Synowicki, R.A.; Hilfiker, J.N. Mueller matrix characterization of flexible plastic substrates. *Appl. Surf. Sci.* **2017**, *421*, 518–528. [CrossRef]
21. Refractive Index Database. Available online: https://refractiveindex.info/?shelf=glassbook=soda-limepage=Rubin-clear (accessed on 9 December 2017).
22. Poudel, K.N. Computational Modeling of Maximum Length Sequence (MLS) Multilayer and Grating Structures. Ph.D. Thesis, Middle Tennessee State University, Murfreesboro, TN, USA, February 2020.
23. Frequency Selective Surface, Periodic Complementary Split Ring Resonator. Available online: https://www.comsol.com/model/download/281491/models.rf.frequencyselective (accessed on 4 December 2017).
24. Fu, X.; Du, Q. Uptake of Di-(2-ethylhexyl) Phthalate of Vegetables from Plastic Film Greenhouses. *J. Agric. Food Chem.* **2011**, *59*, 11585–11588. [CrossRef]
25. Xie, Z.-W.; Yang, J.-H.; Vashistha, V.; Lee, W.; Chen, K.-P. Liquid-crystal tunable color filters based on aluminum metasurfaces. *Opt. Express* **2017**, *25*, 30764–30770. [CrossRef] [PubMed]
26. Lin, M.-Y.; Tsai, T.-H.; Hsiao, L.-J.; Tu, W.-C.; Wu, S.-H.; Wang, L.A.; Lee, S.-C.; Lin, H.Y. Design and Fabrication of Nano-Structure for Three-Dimensional Display Application. *IEEE Photonics Technol. Lett.* **2016**, *28*, 884–886. [CrossRef]
27. Wu, C.-L.; Sung, C.-K.; Yao, P.-H.; Chen, C.-H. Sub-15 nm linewidth gratings using roll-to-roll nanoimprinting and plasma trimming to fabricate flexible wire-grid polarizers with low colour shift. *Nanotechnology* **2013**, *24*, 265301. [CrossRef] [PubMed]
28. Shin, Y.J.; Pina-Hernandez, C.; Wu, Y.-K.; Ok, J.G.; Guo, L.J. Facile route of flexible wire grid polarizer fabrication by an-gled-evaporations of aluminum on two sidewalls of an imprinted nanograting. *Nanotechnology* **2012**, *23*, 344018. [CrossRef]
29. Wu, C.-L.; Yao, P.-H.; Lin, C.-H.; Sung, C.-K.; Chen, C.-H. Fabrication of flexible metallic wire grid polarizer using thermal NIL and lift-off processes. *Microelectron. Eng.* **2012**, *98*, 117–120. [CrossRef]

30. Chen, L.; Wang, J.J.; Walters, F.; Deng, X.; Buonanno, M.; Tai, S.; Liu, X.; Deng, D. 58 nm half-pitch plastic wire-grid polarizer by nanoimprint lithography. *J. Vac. Sci. Technol. B Microelectron. Nanometer Struct.* **2007**, *25*, 2654. [CrossRef]
31. Ahn, S.-W.; Lee, K.-D.; Kim, J.-S.; Kim, S.H.; Park, J.-D.; Lee, S.-H.; Yoon, P.-W. Fabrication of a 50 nm half-pitch wire grid polarizer using nanoimprint lithography. *Nanotechnology* **2005**, *16*, 1874–1877. [CrossRef]